processes

MDPI

Article

Study on the Damage Mechanism of Coal under Hydraulic Load

Hongyan Li [1,2,3], Yaolong Li [1,2], Weihua Wang [2,3,*], Yang Li [2], Zhongxue Sun [2,3], Shi He [2,3] and Yongpeng Fan [2]

[1] School of Mechanics and Engineering, Liaoning Technical University, Fuxin 123000, China
[2] Mine Safety Technology Branch, China Coal Research Institute, Beijing 100013, China; zhongxue13@163.com (Z.S.)
[3] State Key Laboratory of Coal Mine Disaster Prevention and Control, China Coal Research Institute, Beijing 100013, China
* Correspondence: wh1987_wang@163.com

Abstract: Hydraulic fracturing is extensively utilized for the prevention and control of gas outbursts and rockbursts in the deep sections of coal mines. The determination of fracturing construction parameters based on the coal seam conditions and stress environments merits further investigation. This paper constructs a damage analysis model for coal under hydraulic loads, factoring in the influence of the intermediate principal stress, grounded in the octahedron strength theory analysis approach. It deduces the theoretical analytical equation for the damage distribution of a coal medium subjected to small-flow-rate hydraulic fracturing in underground coal mines. Laboratory experiments yielded the mechanical parameters of coal in the study area and facilitated the fitting of the intermediate principal stress coefficient. Leveraging these datasets, the study probes into the interaction between hydraulic loads and damage radius under assorted influence ranges, porosity, far-field crustal stresses, and brittle damage coefficients. The findings underscore that hydraulic load escalates exponentially with the damage radius. Within the variable range of geological conditions in the test area, the effects of varying influence range, porosity level, far-field stress, and brittle damage coefficient on the outcomes intensify one by one; a larger hydraulic load diminishes the impact of far-field stress variations on the damage radius, inversely to the influence range, porosity, and brittle damage. The damage radius derived through the gas pressure reduction method in field applications corroborates the theoretical calculations, affirming the precision of the theoretical model. These findings render pivotal guidance for the design and efficacy assessment of small-scale hydraulic fracturing in underground coal mines.

Keywords: hydraulic fracturing; permeability enhancement; three-parameter failure criterion; intermediate principal stress; damage model; porosity

Citation: Li, H.; Li, Y.; Wang, W.; Li, Y.; Sun, Z.; He, S.; Fan, Y. Study on the Damage Mechanism of Coal under Hydraulic Load. *Processes* **2024**, *12*, 925. https://doi.org/10.3390/pr12050925

Academic Editor: Qingbang Meng

Received: 27 March 2024
Revised: 25 April 2024
Accepted: 26 April 2024
Published: 1 May 2024

1. Introduction

As China's shallow coal resources gradually deplete, the depth of underground mining increases, posing significant challenges for an increasing number of mines faced with deep coal mining issues [1–4]. The original state of in situ stress in coal seams is disrupted by various mining engineering disturbances, manifesting as various forms of stress loading and unloading [5–8]. Currently, strength analyses of coal–rock mass failure primarily utilize the Mohr–Coulomb strength criterion, which ignores the impact of the intermediate principal stress on material strength and is inadequate for describing the strength failure of the underground coal–rock medium under true triaxial stress conditions [9]. Shi [10] introduced the intermediate principal stress coefficient β into the Hoek–Brown criterion, improving the two-dimensional strength criterion to a three-dimensional one. The revised strength criterion has been verified by experiments and compared with three other strength criteria. Zhang [11] established a unified solution for the size of the plastic zone and the stress field before translational impact instability, based on the Unified Strength Theory, finding significant effects of changes in the intermediate principal stress coefficient on coal seam translational impact instability. Adam [12] innovated a generalized method

that transforms two-dimensional failure criteria (i.e., Mohr–Coulomb and Hoek–Brown failure criteria) into three-dimensional criteria to predict true triaxial experimental data. Du [13] demonstrated through experiments that the twin-shear unified strength criterion can accurately describe the strength characteristics of sandstone under different stress paths. Yin [14] believes that the loading or unloading of the intermediate principal stress has a significant impact on the evolution of the original coal permeability, which cannot be ignored in practical conditions. In the high-stress environment of deep coal mining, disasters such as coal and gas outbursts and rockbursts are more likely to occur. Without effective preventive measures, these can significantly impact production and severely limit capacity release [15–17]. Hydraulic fracturing [18–23] and hydraulic slotting [24–28] measures have been applied to more mines and mining group companies, and have proven to be applicable to more coal production enterprises in terms of environmental protection and low risk. Hydraulic fracturing [29,30] is a technique that involves the continuous injection of fluid into the coal–rock medium to induce fractures. This process not only enhances the permeability of the coal–rock medium to facilitate gas extraction but also can cause the fracturing of the overburden to reduce the likelihood of rock bursts. Since the first hydraulic fracturing operation in the United States in 1947, the technology has undergone significant advancements over more than 50 years, evolving from theoretical research to practical field applications.

Due to the unique underground three-dimensional spatial environment of coal seams, the hydraulic measures employed cannot solely focus on increasing hydraulic pressure to enhance regional coal permeability. However, how to reasonably set and match the hydraulic pressure value according to the occurrence of coal and its own properties can currently only be determined based on experiments in the mine, with the determination method having a certain randomness and lag, and thus not providing good preliminary guidance for hydraulic fracturing. Since the coal medium will be damaged and destroyed by external loading, Liu [31] used the Gurson damage model to establish a continuous damage model for hydraulic fracturing, with numerical simulation results showing that the damage zone is mainly concentrated near the perforation, presenting a band-like distribution. Cai [32] conducted numerical simulations of hydraulic fracturing using the multi-porous medium control equation and the cohesive damage model, which were consistent with the observed field influence range. Yi [33] defined a damage variable influenced by the maximum normal stress, with coal permeability changing with damage, and established a fully coupled seepage-damage numerical model. In the field of water inrush from shaft lining, Rong [34] based on the Unified Strength Theory and the Bui elastoplastic damage model, derived the internal stress expression of shaft lining and discussed the impact of porosity and modulus reduction ratio on the critical inrush pressure. Guo [35,36] established a damage constitutive model based on energy dissipation to study the effects of gas pressure on the mechanical properties, permeability, and energy response characteristics of coal–rock composites under true triaxial stress paths. Wei [37] derived the stress equation of rock microelements in the damage and failure zones without ignoring shear stress. Studies on water inrush from both shaft lining and hydraulic fracturing involve fluid–solid coupling problems under loading conditions on circular holes, but they have completely different liquid and solid phase boundary conditions, and therefore the research objects have significant differences in internal stress fields and damage deformation laws.

Previous studies have primarily focused on analyzing the initiation of hydraulic fracturing from the perspective of fracture mechanics, or on qualitatively describing the propagation patterns of fractures. This paper derives the relationship between the damage radius of coal and the hydraulic load considering the intermediate principal stress from the perspective of coal body damage, and provides a theoretical analytical formula to guide field practice. We conducted uniaxial compression tests, triaxial compression experiments, and mercury penetration experiments to determine the mechanical parameters of the coal medium, and substituted the experimentally obtained data into equations to investigate the influence mechanisms of water pressure, porosity, geostress, and their ranges on

coal permeability enhancement during hydraulic fracturing. These findings provide a reference and basis for the design of small-displacement hydraulic fracturing permeability enhancement applications in coal mines.

2. Analysis of Coal–Rock Medium Damage under Hydraulic Loads

Following drilling operations, the redistribution of internal stress within the coal medium leads to the damage of parts of the coal mass, subsequently resulting in the formation of plastic and elastic zones. Assuming that the hydraulic load is uniformly distributed and acts on the interior of the borehole, which has a regular circular shape, let the radius of the borehole be a, the overall influence area radius be b, and the plastic (damage) influence area radius be c. The schematic diagram of the stress around the borehole is illustrated in Figure 1. The surrounding coal medium of the borehole is an isotropic porous medium, with an effective porosity of φ.

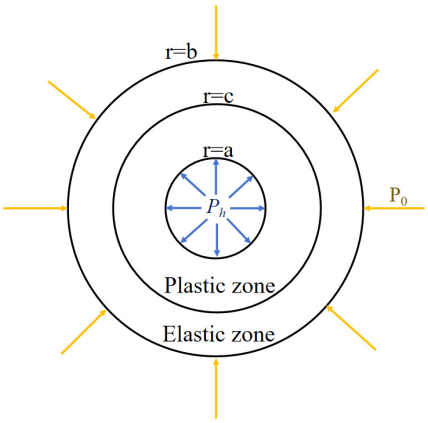

Figure 1. Influence zone of the coal under hydraulic loading.

According to the expression for the damage variable of coal rock defined by Zhou [38], it can be seen that

$$D = \begin{cases} 0 & \varepsilon < \varepsilon_c \\ \left(\frac{\varepsilon}{\varepsilon_t}\right)^n & \varepsilon \geq \varepsilon_c \end{cases} \tag{1}$$

where ε is the strain, ε_c is the peak strain, ε_t is a constant, and n represents the material damage factor. Thus, the constitutive equation for coal–rock medium damage is as follows:

$$\sigma = \begin{cases} E\varepsilon & \varepsilon < \varepsilon_c \\ E\left(1 - \left(\frac{\varepsilon}{\varepsilon_t}\right)^n\right)\varepsilon & \varepsilon \geq \varepsilon_c \end{cases} \tag{2}$$

According to the Lemaitre equivalent strain principle and extending the uniaxial constitutive model to the three-dimensional state, then

$$\sigma_i = E(1 - D')\varepsilon_i,\ D' = \left(\frac{\varepsilon_i}{\varepsilon_t}\right)^n \tag{3}$$

Assuming the coal–rock medium in the plastic zone is incompressible, then the volumetric strain is zero. The equivalent strain of the coal–rock medium in the plastic zone under triaxial conditions is as follows:

$$\begin{aligned} &\varepsilon_i = \frac{\sqrt{2}}{3}\sqrt{(\varepsilon_r - \varepsilon_z)^2 + (\varepsilon_r - \varepsilon_\theta)^2 + (\varepsilon_z - \varepsilon_\theta)^2} \\ &\varepsilon_r + \varepsilon_\theta = 0, \\ &\varepsilon_z = 0 \end{aligned} \tag{4}$$

Considering that the boundary between the elastic and plastic zones is the boundary of damage, the expressions for displacement, strain, and equivalent volumetric strain within the plastic zone under the boundary condition $\varepsilon_i|_{r=c} = \varepsilon_c$ can be obtained as

$$\begin{cases} u = \frac{\sqrt{3}}{2r}c^2\varepsilon_c \\ \varepsilon_r = -\frac{\sqrt{3}}{2r^2}c^2\varepsilon_c,\ \varepsilon_\theta = -\frac{\sqrt{3}}{2r^2}c^2\varepsilon_c,\ \varepsilon_i = \frac{c^2\varepsilon_c}{r^2} \end{cases} \tag{5}$$

From this, the expression for the damage variable D' within the plastic zone in relation to the borehole radius r can be derived as

$$D' = \left(\frac{\varepsilon_c c^2}{\varepsilon_t r^2}\right)^n \tag{6}$$

3. Force Analysis of Hydraulic Loads Acting on the Elastic Zone of the Coal–Rock Medium

Based on the principles of elasticity and Darcy's law, the hydraulic pressure load P_h within the borehole can be obtained as

$$\begin{cases} \frac{d^2p}{dr^2} + \frac{1}{r}\frac{dp}{dr} = 0 \\ p|_{r=a} = p_h,\ p|_{r=b} = 0 \end{cases} \tag{7}$$

Solve the differential equation:

$$p = \frac{p_h}{\ln(a/b)}\ln(r/b) \tag{8}$$

From Equation (8), it can be determined that the permeation force within the coal body under the action of hydraulic load is

$$F = \varphi\frac{dp}{dr} = \varphi\frac{p_h}{r\ln(a/b)} \tag{9}$$

Assuming the stress distribution due to hydraulic load within the borehole is plane-symmetric, with compressive stress being negative and tensile stress being positive, the stress distribution within the elastic zone is as follows:

$$\frac{d\sigma_r}{dr} + \frac{\sigma_r - \sigma_\theta}{r} - F = 0 \tag{10}$$

The deformation of the elastic zone of the coal body is in accordance with Hooke's law, so the constitutive equation of the plane strain problem is

$$\begin{cases} \varepsilon_r = \frac{1-\mu^2}{E}\left(\sigma_r - \frac{\mu}{1-\mu}\sigma_\theta\right) \\ \varepsilon_\theta = \frac{1-\mu^2}{E}\left(\sigma_\theta - \frac{\mu}{1-\mu}\sigma_r\right) \end{cases} \tag{11}$$

The geometric equation is

$$\varepsilon_r = \frac{du}{dr},\ \varepsilon_\theta = \frac{u}{r},\ \gamma_{r\theta} = 0 \tag{12}$$

After substituting Equations (9), (11), and (12) into Equation (10), we can obtain

$$\frac{d^2u}{dr^2} + \frac{1}{r}\frac{du}{dr} - \frac{u}{r^2} = \frac{F}{E}\frac{(1+\mu)(1-2\mu)}{1-\mu} \tag{13}$$

Solving the differential equation in Equation (13) yields

$$u = \frac{\varphi}{2E}\frac{p_h}{\ln(a/b)}\frac{(1+\mu)(1-2\mu)}{1-\mu}r\ln r + C_1 r + \frac{C_2}{r} \tag{14}$$

Therefore, the stress distribution in the elastic zone under the influence of hydraulic loading is as follows:

$$\begin{cases} \sigma_r = \xi\left(\zeta(\ln r + 1 - \mu) + C_1 + \frac{2\mu-1}{r^2}C_2\right) \\ \sigma_\theta = \xi\left(\zeta(\ln r + \mu) + C_1 + \frac{1-2\mu}{r^2}C_2\right) \end{cases} \tag{15}$$

where

$$\zeta = \frac{E}{(1+\mu)(1-2\mu)},\ \zeta = \frac{\varphi}{2E}\frac{p_h}{\ln(a/b)}\frac{(1+\mu)(1-2\mu)}{(1-\mu)}$$

Assuming that the radial stress at the boundary between the elastic and plastic zones is $-\sigma^c{}_r$, the boundary conditions are as follows:

$$\sigma_r|_{r=b} = -P_0,\ \sigma_r|_{r=c} = -\sigma^c{}_r \tag{16}$$

Substituting the boundary conditions into Equation (14) yields its coefficients as

$$\begin{cases} C_1 = \frac{c^2}{b^2-c^2}\left[\left(\frac{(\sigma_r^c - P_0)}{\xi} - \zeta\cdot\ln(b/c)\right)\right] \\ \quad -\zeta(\ln b + 1 - \mu) - \frac{P_0}{\xi} \\ C_2 = \frac{b^2c^2}{b^2-c^2}\left[\frac{(\sigma_r^c - P_0)}{\xi(1-2\mu)} - \frac{\zeta}{1-2\mu}\ln(b/c)\right] \end{cases}$$

4. Force Analysis of Hydraulic Loads Acting on the Plastic Zone of the Coal–Rock Medium

Based on the unified strength theory, it can be inferred that hydraulic loads acting on boreholes can be considered plane strain problems. Assume the intermediate principal stress to be

$$\sigma_z = \sigma_2 = \frac{\beta}{2}(\sigma_1' + \sigma_3'),\ 0 \le \beta \le 1 \tag{17}$$

The coefficient β represents the intermediate principal stress coefficient, and for plastically incompressible materials, β = 1. A comparative analysis of reference [34] indicates that

$$\sigma_1 = \sigma_r';\ \sigma_2 = \sigma_z';\ \sigma_3 = \sigma_\theta';\ \sigma_1 > \sigma_2 > \sigma_3$$

In the equation, σ_i' represents each principal stress within the plastic zone, MPa.

According to the spatial stress theory of regular octahedron in [39], the strength criterion of the coal–rock mass under hydraulic loading in the plastic zone is as follows:

$$\frac{\tau_{oct}}{f_c} + \alpha\frac{\sigma_{oct}}{f_c} + \beta = 0 \tag{18}$$

In the equation, σ_{oct} is the positive stress in the octahedral stress space:
$\sigma_{oct} = \frac{1}{3}(\sigma_1' + \sigma_2' + \sigma_3')$, MPa;
τ_{oct} is the octahedral stress space shear stress:
$\tau_{oct} = \frac{1}{3}\sqrt{(\sigma_1' - \sigma_2')^2 + (\sigma_1' - \sigma_3')^2 + (\sigma_2' - \sigma_3')^2}$, MPa;
α, β are constant coefficients of the equation;
f_c is the uniaxial compressive strength of the coal, MPa.
Simplify Equation (18):

$$\left(\frac{\sqrt{6}}{6f_c} + \frac{\alpha}{2f_c}\right)\sigma_r' - \left(\frac{\sqrt{6}}{6f_c} - \frac{\alpha}{2f_c}\right)\sigma_\theta' + \beta = 0 \tag{19}$$

Assign $A = \frac{\sqrt{6}}{6f_c} + \frac{\alpha}{2f_c}$, $B = \frac{\sqrt{6}}{6f_c} - \frac{\alpha}{2f_c}$, and then

$$A\sigma_r' - B\sigma_\theta' + \beta = 0 \tag{20}$$

Assuming that the damage in the plastic zone of the coal is isotropic, the axial and circumferential stresses satisfy the following relation:

$$\sigma_r' = \frac{\sigma_r}{1-D'},\ \sigma_\theta' = \frac{\sigma_\theta}{1-D'}$$

It is possible to derive a strength criterion for the plastic zone of coal and rock under hydraulic loading:

$$A\sigma_r - B\sigma_\theta + \beta\left(1 - \left(\frac{c^2\varepsilon_c}{\varepsilon_t r^2}\right)^n\right) = 0 \tag{21}$$

Assign $\omega_1 = \frac{B-A}{B}$, $\omega_2 = \frac{\beta}{B}$, $\omega_3 = \left(\frac{c^2\varepsilon_c}{\varepsilon_t}\right)^n$, and the above equation can be transformed by substituting it into the balanced Equation (10):

$$\sigma_r = C_1 r^{-\omega_1} + \frac{\omega_2\omega_3}{2n-\omega_1} r^{-2n} + \frac{\omega_2}{\omega_1} + \frac{\varphi p_h}{\omega_1 \ln(a/b)} \tag{22}$$

Combined with the boundary condition $\sigma_r|_{r=a} = -p_h$, Equation (22) can be solved to finally obtain the radial and circumferential stresses in the plastic zone of the coal–rock medium under hydraulic loading:

$$\begin{cases} \sigma_r = -a^{\omega_1}\left[\frac{\omega_2\omega_3}{2n-\omega_1}a^{-2n} + \frac{\omega_2}{\omega_1} + p_h\left(1 + \frac{\varphi}{\omega_1\ln(a/b)}\right)\right] r^{-\omega_1} \\ \qquad + \frac{\omega_2\omega_3}{2n-\omega_1} r^{-2n} + \frac{\omega_2}{\omega_1} + \frac{\varphi p_h}{\omega_1\ln(a/b)} \\ \sigma_\theta = \frac{A\sigma_r + \beta\left[1-\omega_3 r^{-2}\right]}{B} \end{cases} \tag{23}$$

At the boundary between the elastic and plastic zones within the coal affected by the hydraulic load, the radial stress in the plastic zone is equal to the radial stress in the elastic zone, which is

$$\sigma^e{}_r|_{r=c} = \sigma^p{}_r|_{r=c} \tag{24}$$

Meanwhile, the damage variable at the boundary is 0, that is, $D' = 0$. Since the stresses in the elastic and plastic zones are equal, substituting the stress expression at $r = c$ presented in Equation (15) and $D' = 0$ into the strength criterion in Equation (21) yields

$$A\sigma^e{}_r|_{r=c} - B\sigma^e{}_r|_{r=c} + \beta = 0 \tag{25}$$

Joining the above two equations yields the following equation:

$$p_h = \frac{\omega_1\gamma_3\ln(a/b)\left[\begin{array}{l}\gamma_3\left(1-\frac{\gamma_4}{a^2}\right)^n + \gamma_2(1-\gamma_4) \\ -\frac{\omega_5\left[Bc^2+b^2(2\mu-1)\right]}{\gamma_3}\end{array}\right]}{\omega_1\gamma_2\gamma_3 + \varphi\left[\begin{array}{l}\gamma_1\gamma_4 + B\gamma_3\gamma_5(\ln c + \mu - 1) - c^2B\gamma_5\cdot \\ \ln\left(b^2/c + 1 - \mu\right) + (2\mu-1)b^2\gamma_5\ln(b/c)\end{array}\right]} \tag{26}$$

γ_1, γ_2, γ_3, γ_4, γ_5, ω_5 in the equation are determined by the following equations:

$$\begin{aligned} \gamma_1 &= \tfrac{\omega_2\omega_3}{\omega_1-1} \\ \gamma_2 &= \tfrac{\omega_2}{\omega_1} \\ \gamma_3 &= b^2 - c^2 \\ \gamma_4 &= a^{\omega_1}c^{\omega_1} \\ \gamma_5 &= \omega_1\omega_4, \\ \omega_4 &= \tfrac{(1+\mu)(1-2\mu)}{2E(1-\mu)} \\ \omega_5 &= \tfrac{\sigma^c{}_r(1+\mu)}{E} \end{aligned}$$

Under certain conditions of fixed compressive strength, porosity, brittleness index, and damage factor for the coal or rock, the analytical solution for the radius of influence in the coal–rock medium zone under the action of hydraulic load within a borehole can be derived from the above theoretical analysis. Similarly, the radius of the damage zone under the influence of hydraulic load can also be determined.

5. Analysis of the Mechanism of Coal Damage under Hydraulic Load

5.1. Analyzing the Mechanism of Hydraulic Load Damage through Theoretical Analysis

5.1.1. Laboratory Determination of Coal's Physical Dynamics Parameters

To analyze the mechanisms of hydraulic-load-induced damage through analytical solutions derived from the aforementioned theoretical derivations, and to guide the field practices at Yangmei Wukuang in Shanxi, China, experiments were conducted on coal samples from the mine. These included uniaxial compressive loading tests, triaxial compressive loading tests, and porosity determination experiments to measure their mechanical parameters.

Two larger coal samples were extracted from the coal face, and four cores were taken from each piece. These cores were processed into cylinders of 50 × 100 mm and polished to ensure flatness at both ends. Then, 10 g of cinder was carved with a knife at each of the four different locations on the original coal and kept for later.

The TAW-2000 electro-hydraulic servo testing machine was employed for uniaxial compression tests with a displacement loading method at a rate of 0.1 mm/min. Axial and radial displacements were measured by an extensometer, and a computer was used to record data on loads, stresses, strains, and displacements during the test. Four experimental groups were set up for the uniaxial experiments, with all samples derived from the same coal seam. The measured mechanical parameters are shown in Table 1, and the stress–strain curves for the four samples are depicted in Figure 2. These curves show some differences, especially the one from sample #4. In fact, coal is a highly heterogeneous rock. It has low material strength and a rich pore structure, which leads to the easy formation of cracks and defects under the influence of strata movement and mining disturbances. These cracks and defects are the reasons for the differences in the stress–strain curves. The trends of curves #1, #2, and #3 are more consistent with the ideal full stress–strain curves of rocks. Sample #4 has natural joint planes, and when the stress reached 9.13 MPa, it underwent large-scale fracturing, causing a sudden change in the curve. The average results of the four tests indicate that the coal body's modulus of elasticity E = 1820 MPa, Poisson's ratio μ = 0.32, and uniaxial compressive strength f_c = 10.52 MPa, with the hydraulic fracturing drilling radius being 0.047 m.

Table 1. Partial mechanical parameters of the coal.

Specimen Number	f_c/Mpa	E/GPa	μ
1#	11.47	1.93	0.307
2#	10.88	2.52	0.341
3#	10.59	1.18	0.321
4#	9.12	1.66	0.319
avg	10.52	1.82	0.322

The damage coefficients $\varepsilon_c/\varepsilon_t$ and n have a corresponding relationship in Equation (6), and the constant ε_t value was obtained by using the method described in reference [38]. Using MATLAB R2022a, the full stress–strain curve data obtained from the uniaxial compression test were input into the damage constitutive equation to fit the corresponding value of n. Combining the peak strain ε_c, the $\varepsilon_c/\varepsilon_t$ and n values for the four specimens were statistically analyzed to fit the relationship curve between $\varepsilon_c/\varepsilon_t$ and n, as illustrated in Figure 3.

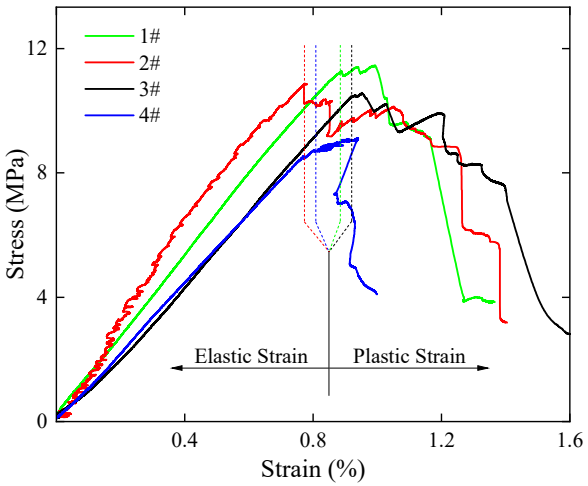

Figure 2. Stress–strain curve of coal.

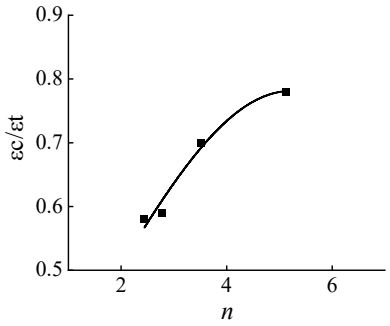

Figure 3. Coefficient curve of $\varepsilon_c/\varepsilon_t$ vs. n.

Triaxial compression tests were conducted on the GCTS RTR-4600 high-performance rock mechanics testing system at the National Key Laboratory for CCRI. Four experimental groups were established, with confining pressures set at 5 MPa, 15 MPa, 20 MPa, and 25 MPa, respectively (Figure 4). During the experiments, the confining pressure was first increased to the set value at a rate of 50 KPa/s, followed by axial pressure at the same rate until specimen failure, recording the peak axial stress at failure. By fitting Equation (18) with the obtained three principal stresses under triaxial stress conditions (as shown in Table 2) and the uniaxial compressive strength of the coal specimen f_c = 10.52 MPa, the equation constants α = 0.3413, β = −0.1231 were obtained.

Table 2. Results of triaxial compression coal bursting test.

Specimen Number	σ_1 /MPa	σ_2 /MPa	σ_3 /MPa	$\frac{\sigma_{oct}}{f_c}$	$\frac{\tau_{oct}}{f_c}$
SS-01	−14.83	−5.00	−5.00	−1.01	0.57
SS-02	−29.87	−15.00	−15.00	−1.91	0.94
SS-03	−43.00	−20.00	−20.00	−3.39	1.33
SS-04	−53.40	−25.00	−25.00	−4.22	1.64

Porosity determination experiments were carried out using the PoreMaster GT-60 mercury intrusion porosimeter (Quantachrome Instruments, Boynton Beach, FL, USA). Samples were collected by carving particles of 1–3 mm in size from the original coal specimens with a knife. The pore volume distribution density function of the four groups of samples is depicted in Figure 5, and the corresponding porosity values are listed in Table 3, with an average porosity of φ = 12.6%.

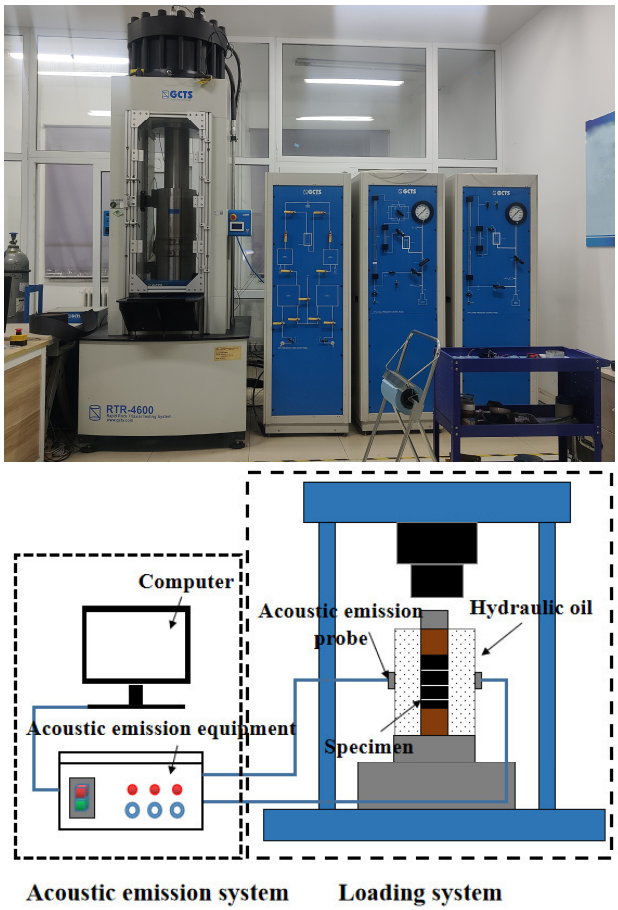

Figure 4. GCTS RTR-4600 high-performance rock mechanics testing system and schematic diagram.

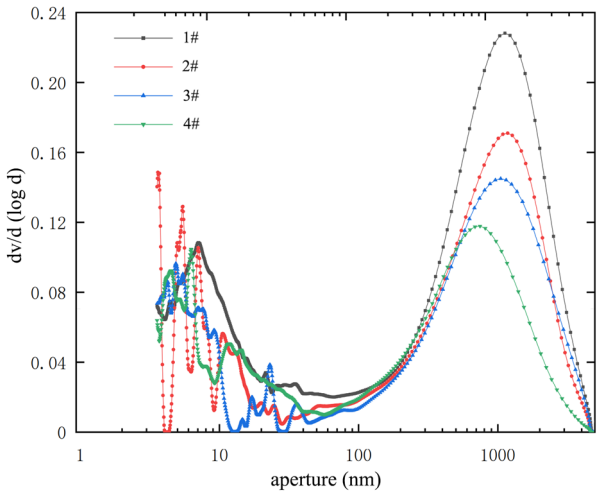

Figure 5. Pore volume distribution density function diagram.

Table 3. Porosity distribution table.

	1#	2#	3#	4#
Porosity/%	10.22	14.42	14.47	11.32
Adsorption pore/%	3.30	3.44	4.28	3.75
Seepage pore/%	6.92	10.98	10.19	7.57

5.1.2. Effect of Hydraulic Water Pressure on Damage Radius at Different Influence Ranges

The damage radius under different hydraulic pressure conditions can be obtained from Equation (26), as illustrated in Figure 6. The enlarged views at locations c = 1 and c = 1.2 are shown in Figures 6b and 6c, respectively. As indicated in the figure, within the same influence range, the required hydraulic load exhibits an exponential growth trend as the damage radius of the coal mass increases. Under the same damage radius condition, as the influence range expands, the gradient of hydraulic pressure change shows a slightly increasing trend. This implies that the larger the influence range, the greater the hydraulic pressure needed to cause the same degree of damage. When the damage radius is set at 1 m and the influence ranges exerted by the hydraulic load on the coal are 2 m, 3 m, and 4 m, respectively, the required hydraulic pressures will be 12.6 MPa, 13.1 MPa, and 13.2 MPa. When the damage radius is set at 1.2 m and the influence range is the same, the hydraulic pressures needed are 48.1 MPa, 49.4 MPa, and 49.8 MPa. As depicted in Figure 7, under a fixed damage radius, the greater the zone of influence, the smaller the incremental increase in the required water pressure. Comparing the cases of damage radii of 1 m and 1.2 m laterally, it is obvious that the larger the damage radius, the more pronounced the effect of the influence range on the hydraulic pressure.

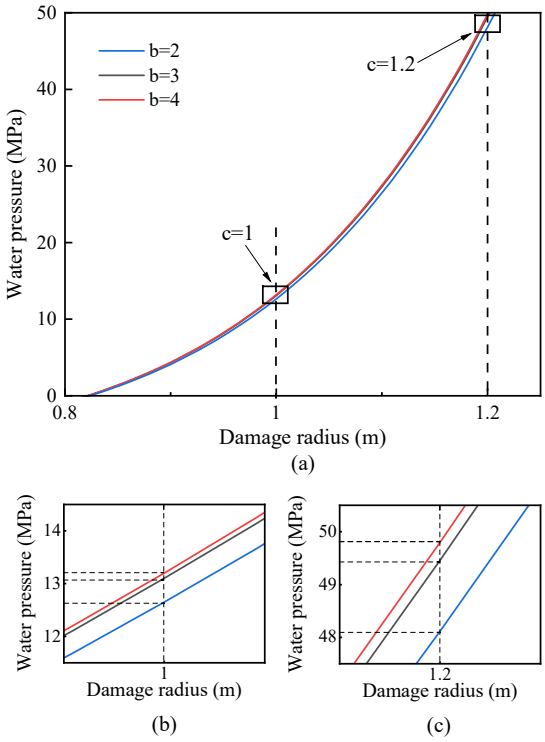

Figure 6. Curve of damage radius c versus hydraulic water pressure P_h for different influence ranges c (**a**), and local magnification diagrams at c = 1 m (**b**) and c = 1.2 m (**c**).

The maximum pressure of the mud pump car matched with the drilling rig is generally 15 MPa, but it can reach 20 MPa when pumping with small flow, while the maximum pressure of the dedicated fracturing pump car underground can reach 50 MPa at present. In the practical application of low-displacement hydraulic fracturing in coal mines, measures that solely consider increasing water pressure to promote coal fracturing and expand the range of influence have limited effects on the permeability enhancement of coal subject to triaxial stress conditions. With known basic mechanical parameters of the coal, one can nearly match the hydraulic pressure parameters for the implementation of hydraulic fracturing and the corresponding damage and influence range in the coal. This provides guidance and reference for the design and evaluation of the effectiveness of small-displacement hydraulic fracturing applied in coal mines underground.

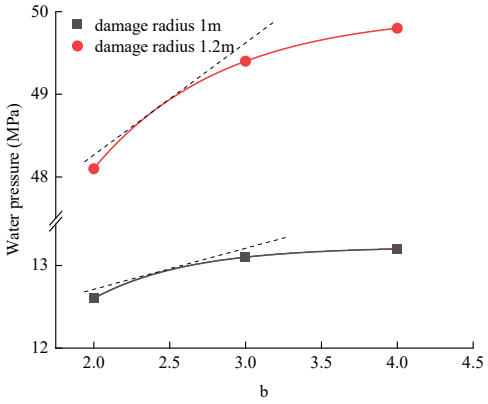

Figure 7. Relation between influence range and hydraulic pressure.

5.1.3. Effect of Hydraulic Water Pressure on Damage Radius at Different Porosity Levels

It is generally believed that the porosity of the same coal seam is a fixed value. However, as roadways are excavated, the surrounding rock around the roadways develops cracks and expands under crustal stress, leading to changes in its internal porosity, which is related to coal strain or deformation [40,41]. When hydraulic fracturing boreholes are arranged perpendicular to the roadway walls of the coal seam, the porosity of the coal at different depths of the boreholes varies slightly. Taking the results of the porosity determination experiments as intervals, the porosity was set as φ = 0.08, 0.10, 0.12, and 0.14. The relationship between the damage radius c and hydraulic water pressure P_h for different porosities φ at an influence range of 2 m is calculated and plotted, and the curves are shown in Figure 8. Among them, Figures 8b and 8c are the enlarged plots at the positions of P_h = 15 MPa and P_h = 45 MPa, respectively.

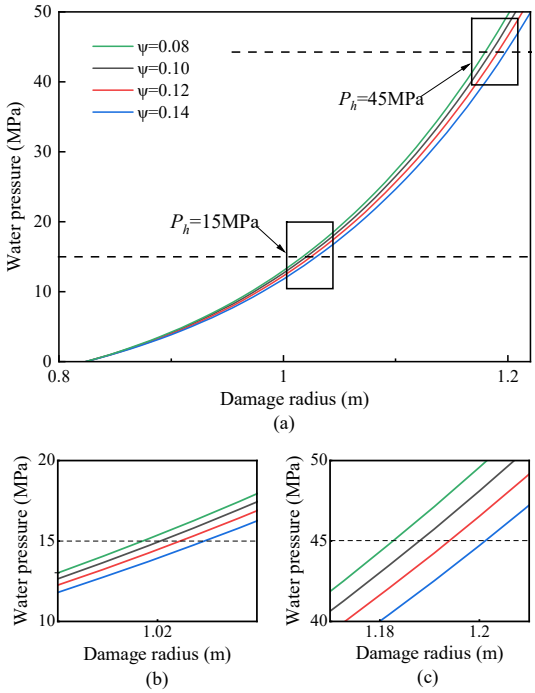

Figure 8. Curve of damage radius c versus hydraulic water pressure P_h for different porosity values φ (**a**), and local magnification diagrams at P_h = 15 MPa (**b**) and P_h = 45 MPa (**c**).

The observation in Figure 8 reveals that, when P_h is held constant, an increase in coal porosity means more extensive development of internal micro-cracks, which consequently reduces the seepage resistance loss of fracturing fluid inside the pores. This results in

higher pressure accumulation at the crack tip. The macroscopic appearance is that the damage radius increases with increasing porosity. Specifically, for P_h = 15 MPa, the damage radii corresponding to four different porosity values are 1.016 m, 1.020 m, 1.024 m, and 1.028 m, respectively, while for P_h = 45 MPa, they are measured as 1.182 m, 1.188 m, 1.194 m, and 1.201 m, respectively. It can be inferred that during hydraulic fracturing aimed at enhancing permeability, greater water ingress occurs within coal's internal micro-cracks and micropores due to increased porosity levels. This intensifies the coupling between the seepage field and the deformation field, ultimately leading to reduced mechanical properties of coal. The effect of porosity on the damage radius is roughly linear, and better penetration can be obtained by fracturing near the mouth of the hole or in the fracture zone of the coal seam; this phenomenon will be more obvious if the fracturing pressure is increased.

5.1.4. Effect of Hydraulic Water Pressure on Damage Radius at Different Far-Field Crustal Stresses P_0

The far-field crustal stress P_0 is taken as 7 MPa, 11 MPa, and 15 MPa, and the porosity is taken as the average value of φ = 0.126. The curves of the damage radius c versus hydraulic water pressure P_h for different far-field crustal stresses P_0 are plotted as shown in Figure 9.

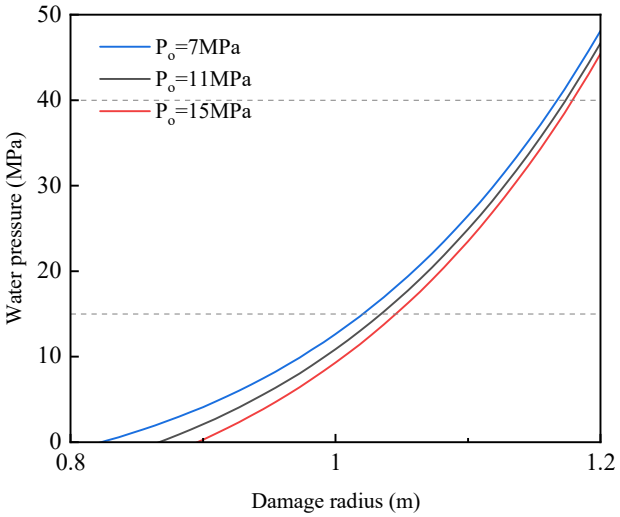

Figure 9. Curve of damage radius c versus hydraulic water pressure P_h for different far-field crustal stresses P_0.

The increase in P_0 from 7 MPa to 15 MPa produced a larger damage radius at the same water pressure. Fracturing with a water pressure of 15 MPa in coal seams under far-field crustal stress of 7 MPa, 11 MPa, and 15 MPa resulted in damage radii of 1.045 m, 1.036 m, and 1.018 m, respectively. Damage radii of 1.189 m, 1.123 m, and 1.083 m were obtained from fractures with a water pressure of 40 MPa in coal seams under far-field crustal stresses of 7 MPa, 11 MPa, and 15 MPa.

In the practice of hydraulic fracturing, the deformation and damage of the surrounding rock around the borehole can simply be considered as a result of a combination of far-field crustal stress, induced stresses, and pore pressures. Higher far-field crustal stress produces wider and more damaged plastic zones for pore water intrusion. But at the same time, for the coal in the elastic zone, its cracks are compressed more densely, and fracturing is more difficult. This is why the effect of far-field crustal stress on the damage radius is larger when the hydraulic pressure is lower, while the effect of far-field crustal stress on the damage radius is relatively smaller when the hydraulic pressure is higher. In addition, when fracturing under high far-field crustal stress, the fracture initiation pressure is greater,

more energy is accumulated, and the fracture extends further after initiation to produce a larger damage radius.

5.1.5. Effect of Hydraulic Water Pressure on Damage Radius for Different Brittle Damage Coefficients n

The value of porosity was taken as an average value of $\varphi = 0.126$. The far-field crustal stress P_0 is 7 MPa. To obtain the equivalent $\varepsilon_c/\varepsilon_t$, the constant n is taken as 3, 3.5, and 4 and substituted into Figure 3. The results are obtained by substituting the data into Equation (26) to plot the relationship curves between the damage radius c and the hydraulic pressure P_h under various brittleness damage coefficients n, as displayed in Figure 10.

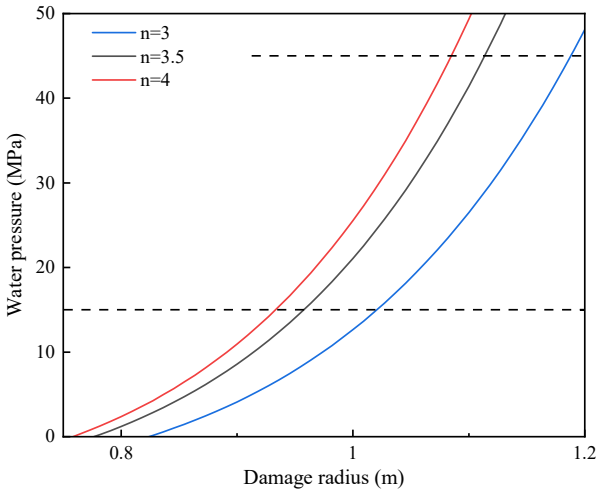

Figure 10. Curve of damage radius c versus hydraulic water pressure P_h for different n.

Constant n represents the brittleness of the coal. The greater n, the denser the coal, and the greater the tendency to undergo elastic deformation and accumulate energy under external load. As shown in the figure, the process from $n = 3$ to 4 resulted in a smaller damage radius at the same water pressure. Fracturing in $n = 3$, $n = 3.5$, and $n = 4$ coals with 15 MPa water pressure resulted in damage radii of 1.045 m, 1.036 m, and 1.018 m, respectively, with 6.0% and 8.2% reductions in damage radius for the $n = 3.5$ and $n = 4$ conditions relative to the $n = 3$ condition. Fracturing in $n = 3$, $n = 3.5$, and $n = 4$ coals with 45 MPa water pressure resulted in damage radii of 1.189 m, 1.123 m, and 1.083 m, respectively, with an increase in damage radius of 6.5% and 10.4% for the $n = 3.5$ and $n = 4$ conditions relative to the $n = 3$ condition. Therefore, compared with the other conditions mentioned above, the influence of different n values on the damage radius is greater, and the higher the water pressure, the greater the influence of n values.

5.2. Practical Validation Study of the Range of Hydraulic Load Damage Effects

The test area is located at No. 15 coal seam 15311, Yangmei Wukuang, Shanxi Province, with an average thickness of 5.12 m, a coal seam permeability coefficient of 0.156 m^2/(MPa-d), a coal sturdiness factor of 0.45, a gas flow attenuation coefficient of 0.329 and gas pressure of 0.5 MPa. According to the Coal Mine Gas Drainage Specification, the coal seam in which the test is carried out belongs to the category of coal seams with high gas extraction difficulties. The mechanical parameters of coal are detailed in Section 5.1.

Five gas pressure measurement boreholes were pre-positioned in the hydraulic fracturing test area with spacing of 0.5 m, 1.0 m, 1.5 m, 2.0 m, and 2.5 m, respectively. Hydraulic fracturing was performed at a hydraulic fracturing borehole after the pressure measured in the boreholes stabilized. During the test, the water pressure was set to 5 MPa, and then increased to 10 MPa after confirmation of sealing, stabilizing for 5 minutes. If there is no leakage from the surrounding boreholes, the pressure will gradually increase to 4 MPa for each layer and 2 min for each layer, until the surrounding boreholes return water steadily,

with a final extreme water pressure of 35.2 MPa. The ultimate purpose of the hydraulic fracturing is to establish a smoother gas seepage network, improve the permeability of the coal seam, and enhance the regional gas extraction effect. Therefore, borehole gas pressure is an important evaluation index for evaluating hydraulic fracturing damage. The pressure gauges were installed in the gas pressure measurement boreholes to monitor and record the pressure status of the pressure measurement point after hydraulic penetration enhancement. The pressures at each pressure measurement point after the implementation of hydraulic penetration enhancement are shown in Figure 11. The gas pressure decrease ratio of the pressure measurement boreholes is shown in Figure 12. After comprehensively analyzing the proportion of gas pressure decrease after 70 days of pumping in the permeability enhancement area, basically, the proportion of gas pressure decrease decreases with the increase in the distance from the borehole of the hydraulic fracturing. Within this, the biggest decrease ratio is 17.8% in borehole #3. It is considered that the decrease in gas pressure by more than 15% is the critical condition for the determination of the damage impact radius. Under the condition of hydraulic pressure of 35.2 MPa, the limit value of the coal damage radius is 1.5 m. The data obtained from the field practice are the same as the limit value of the coal damage radius calculated theoretically under the same condition, which further verifies the correctness of the theoretical analytical formula obtained.

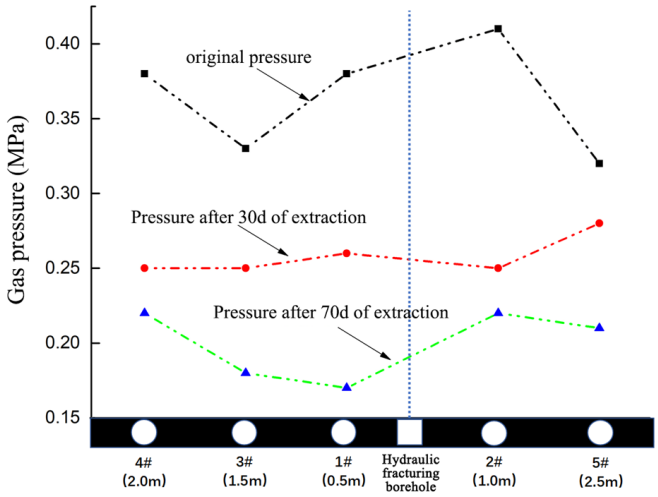

Figure 11. Examination of the coal body influence range by the pressure-drop method.

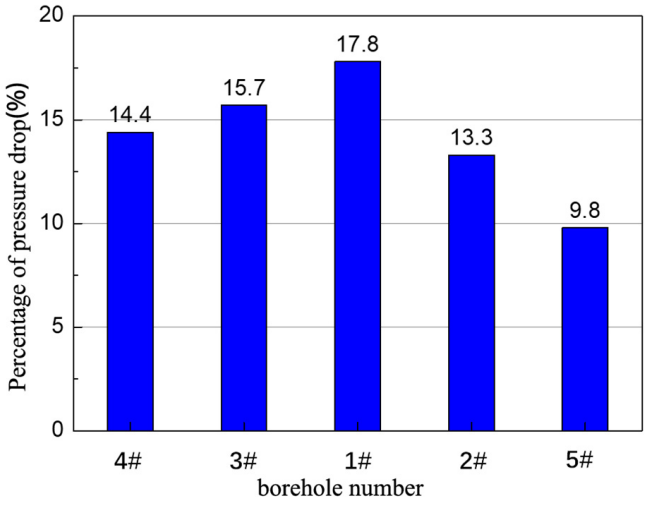

Figure 12. Proportional decline in gas pressure around the drilling hole, measured by hydraulic fracturing.

6. Conclusions

(1) A theoretical analysis has been established to determine the relationship between the damage radii of coal bodies under hydraulic loads, considering the intermediate principal stress and water pressure. This provides a design and reference for the application of small-flow-rate hydraulic fracturing in coal mines to enhance permeability.

(2) A quantitative analysis was conducted based on the in situ conditions of the coal seam, examining the relationship between hydraulic load, damage radius, and the area of influence, which revealed the impact mechanisms of hydraulic fracturing involving water pressure, porosity, geostress, and the range of influence on coal seam permeability enhancement. The experimental results show that the hydraulic load increases exponentially with the damage radius, indicating that continuously increasing the water pressure when it is already high does not yield better results. Within the range of geological conditions in the test area, different areas of influence and porosity levels have a limited impact on the results, while far-field geostress, particularly the brittle damage coefficient, plays a significant role in controlling the damage radius. The effectiveness of hydraulic fracturing is greatly influenced by the stress conditions and rock properties of the coal seam; the larger the hydraulic load, the less the change in far-field stress affects the damage radius, whereas the area of influence, porosity, and brittle damage coefficient have the opposite effect.

(3) The theoretical analysis's findings on the damage range have been validated through data analyses of field measurements, thereby proving the accuracy and feasibility of designing hydraulic fracturing pressure based on theoretical analysis.

Author Contributions: Methodology, H.L.; validation, Z.S.; formal analysis, Y.F.; writing—original draft, W.W.; writing—review & editing, Y.L. (Yaolong Li); visualization, S.H.; funding acquisition, Y.L. (Yang Li). All authors have read and agreed to the published version of the manuscript.

Funding: Supported by the National Natural Science Foundation of China (52304225) and the Technology Innovation Fund of China coal Research Institute (2023CX-I-05).

Data Availability Statement: The original contributions presented in the study are included in the article, further inquiries can be directed to the corresponding author.

Conflicts of Interest: The authors declare no conflict of interest.

References

1. He, M.; Wu, Y.; Gao, Y.; Tao, Z. Research progress of rock mechanics in deep mining. *J. China Coal Soc.* **2024**, *49*, 75–99. [CrossRef]
2. Zhang, Z.; Xie, H.; Zhang, R.; Zhang, Z.; Gao, M.; Jia, Z.; Xie, J. Deformation Damage and Energy Evolution Characteristics of Coal at Different Depths. *Rock Mech. Rock Eng.* **2018**, *52*, 1491–1503. [CrossRef]
3. Siwek, S. Earth tides and seismic activity in deep coal mining. *Int. J. Rock Mech. Min. Sci. Géoméch. Abstr.* **2021**, *148*, 104972. [CrossRef]
4. Ranjith, P.; Zhao, J.; Ju, M.; De Silva, R.V.; Rathnaweera, T.; Bandara, A.K. Opportunities and Challenges in Deep Mining: A Brief Review. *Engineering* **2017**, *3*, 546–551. [CrossRef]
5. Zhou, H.-W.; Liu, J.-F.; Gao, F.; Zhang, R.; Xue, D.-J.; Zhang, Y. Mining-induced mechanical behavior in coal seams under different mining layouts. *J. China Coal Soc.* **2011**, *36*, 1067–1074. [CrossRef]
6. Xie, H.; Lu, J.; Li, C.; Li, M.; Gao, M. Experimental study on the mechanical and failure behaviors of deep rock subjected to true triaxial stress: A review. *Int. J. Min. Sci. Technol.* **2022**, *32*, 915–950. [CrossRef]
7. Wang, K.; Zhao, E.; Guo, Y.; Du, F.; Ding, K. Effect of loading rate on the mechanical and seepage characteristics of gas-bearing coal–rock and its mechanical constitutive model. *Phys. Fluids* **2024**, *36*, 026606. [CrossRef]
8. Li, C.; Wang, S.; You, Q.; Yu, C. A New Measurement of Anisotropic Relative Permeability and Its Application in Numerical Simulation. *Energies* **2021**, *14*, 4731. [CrossRef]
9. Palchik, V. Application of Mohr–Coulomb failure theory to very porous sandy shales. *Int. J. Rock Mech. Min. Sci. Géoméch. Abstr.* **2006**, *43*, 1153–1162. [CrossRef]
10. Shi, X.; Li, Q.; Liu, J.; Gao, L.; Xiao, Z. An Improved True Triaxial Hoek–Brown Strength Criterion. *Adv. Eng. Sci.* **2023**, *55*, 214–221. [CrossRef]
11. Zhang, C.; Qi, H.; Cai, M.; Gao, B. Instability solution of translatory coal seam bumps based on the unified strength theory. *J. China Coal Soc.* **2019**, *44*, 2589–2595. [CrossRef]

12. Schwartzkopff, A.K.; Sainoki, A.; Bruning, T.; Karakus, M. A conceptual three-dimensional frictional model to predict the effect of the intermediate principal stress based on the Mohr–Coulomb and Hoek–Brown failure criteria. *Int. J. Rock Mech. Min. Sci. Géoméch. Abstr.* **2023**, *172*, 105605. [CrossRef]
13. Du, J.; Li, W.; Feng, G.; Wang, Z.; Zhang, H. A study of a true triaxial unloading damage intrinsic model for sand-stone based on the double shear unified strength criterion. *Chin. J. Rock Mech. Eng.* **2024**, *47*, 1–11. [CrossRef]
14. Yin, G.; Liu, Y.; Li, M.; Deng, B.; Liu, C.; Lu, J. Influence of true triaxial loading-unloading stress paths on mechanical property and permeability of coal. *J. China Coal Soc.* **2018**, *43*, 131–136. [CrossRef]
15. He, M.; Wang, Q. Rock dynamics in deep mining. *Int. J. Min. Sci. Technol.* **2023**, *33*, 1065–1082. [CrossRef]
16. Wang, G.; Guo, Y.; Wang, P.; Li, W.; Wu, M.; Sun, L.; Cao, J.; Du, C. A new experimental apparatus for sudden unloading of gas-bearing coal. *Bull. Eng. Geol. Environ.* **2019**, *79*, 857–868. [CrossRef]
17. Patyñska, R.; Kabiesz, J. Scale of seismic and rock burst hazard in the Silesian companies in Poland. *Min. Sci. Technol.* **2009**, *19*, 604–608. [CrossRef]
18. Kang, H.; Feng, Y. Hydraulic fracturing technology and its applications in strata control in underground coal mines. *Coal Sci. Technol.* **2017**, *45*, 1–9. [CrossRef]
19. Chen, D. Gas extraction technology with long borehole segmented hydraulic fracturing in medium-hard coal seam of Binchang mining area. *Coal Eng.* **2023**, *55*, 72–77.
20. Hu, Q.; Liu, L.; Li, Q.; Wu, Y.; Wang, X.; Jiang, Z.; Yan, F.; Xu, Y.; Wu, X. Experimental investigation on crack competitive extension during hydraulic fracturing in coal measures strata. *Fuel* **2020**, *265*, 117003. [CrossRef]
21. Zou, Y.; Gao, B.; Ma, Q. Investigation into Hydraulic Fracture Propagation Behavior during Temporary Plugging and Diverting Fracturing in Coal Seam. *Processes* **2022**, *10*, 731. [CrossRef]
22. Sherratt, J.; Haddad, A.S.; Rafati, R. Modifying the orientation of hydraulically fractured wells in tight reservoirs: The effect of in-situ stresses and natural fracture toughness. *Géoméch. Energy Environ.* **2023**, *36*, 100507. [CrossRef]
23. Manjunath, G.; Liu, Z.; Jha, B. Multi-stage hydraulic fracture monitoring at the lab scale. *Eng. Fract. Mech.* **2023**, *289*, 109448. [CrossRef]
24. Shen, C.-M.; Wang, D.; Zhang, L.; Guo, J.X.; Lin, B.Q. Mechanism and application of inducing high-gas coal out-burst from borehole by waterjet slotting. *J. China Coal Soc.* **2015**, *40*, 2097–2104. [CrossRef]
25. Zheng, S.; Fan, J.; Wang, G.; Wang, E. Study on high efficient gas drainage technology of directional fracturing by cutting slots in steep coal seam. *Coal Sci. Technol.* **2021**, *49*, 112–117. [CrossRef]
26. Lin, B.; Yan, F.; Zhu, C.; Zhou, Y.; Zou, Q.; Guo, C.; Liu, T. Cross-borehole hydraulic slotting technique for preventing and controlling coal and gas outbursts during coal roadway excavation. *J. Nat. Gas Sci. Eng.* **2015**, *26*, 518–525. [CrossRef]
27. Yang, W.; Lin, B.; Gao, Y.; Lv, Y.; Wang, Y.; Mao, X.; Wang, N.; Wang, D.; Wang, Y. Optimal coal discharge of hydraulic cutting inside coal seams for stimulating gas production: A case study in Pingmei coalfield. *J. Nat. Gas Sci. Eng.* **2016**, *28*, 379–388. [CrossRef]
28. Sun, Z.; Liu, Y.; Qi, Q.; Chai, J.; Gu, B. The Influence of High-Pressure Water Jet Cutting Parameters on the Relief of Pressure around the Coal Slot. *Processes* **2023**, *11*, 2071. [CrossRef]
29. Tanner, D.C.; Brandes, C. Understanding Faults: Detecting, Dating, and Modeling. In *Understanding Faults: Detecting, Dating, and Modeling*; Elsevier: Berlin/Heidelberg, Germany, 2019.
30. Ahamed, M.A.; Perera, A.; Li, P.Y.; Ranjith, P.G.; Matthai, S.K. Proppant damage mechanisms in coal seam reservoirs during the hydraulic fracturing process: A review. *Fuel* **2019**, *253*, 615–629. [CrossRef]
31. Liu, J.; Du, G.; Xue, Q. Discussion on Continuum Damage Model of Hydraulic Fracturing. *J. Mech. Strength* **2004**, *26*, 134–137. [CrossRef]
32. Cai, F.; Liu, Z. Simulation and experimental research on upward cross-seams hydraulic fracturing in deep and low-permeability coal seam. *J. China Coal Soc.* **2016**, *41*, 113–119. [CrossRef]
33. Yi, L.-P.; Li, X.-G.; Yang, Z.-Z.; Waisman, H. A fully coupled fluid flow and rock damage model for hydraulic fracture of porous media. *J. Pet. Sci. Eng.* **2019**, *178*, 814–828. [CrossRef]
34. Wang, X.; Cai, H.; Cheng, H. Analysis of shaft lining water irruption mechanism in coal mine based on fluid-solid coupling theory. *J. China Coal Soc.* **2011**, *36*, 2102–2108. [CrossRef]
35. Guo, Y.; Wang, K.; Du, F.; Guo, H.; Li, K.; Wang, Y. Mechanical-permeability characteristics of composite coal rock under different gas pressures and damage prediction model. *Phys. Fluids* **2024**, *36*, 036615. [CrossRef]
36. Wang, K.; Guo, Y.; Wang, G.; Du, F. Seepage and mechanical failure characteristics of gas-bearing composite coal–rock under true triaxial path. *J. China Coal Soc.* **2023**, *48*, 226–237. [CrossRef]
37. Wei, M. Research on the Borehole Wall In-situ Stress Distribution and Stability Based on Damage Mechanics. Master's Thesis, Northeast University of Petroleum, Daqing, China, 2014.
38. Zhou, W.; Yan, G.; Yang, R. Elasto brittle damage model for rockmass based on field tests in Laxiwa arch dam site. *Chin. J. Geotech. Eng.* **1998**, *20*, 57–60.
39. Yu, M.; Liu, J.; Oda, Y.; Gao, J. On Basic Characteristics and Innovation of Yield Criteria for Geomaterials. *Chin. J. Rock Mech. Eng.* **2007**, *26*, 1745–1757.

40. Wu, G.; Chen, W.; Tan, X.; Dai, Y. Effect of the permeability dynamic evolution of saturated rock on the stability of diversion tunnels. *Chin. J. Rock Mech. Eng.* **2020**, *39*, 2172–2182. [CrossRef]
41. Tao, Y.Q.; Xu, J.; Peng, S.J.; Yuan, M. Experimental study of influencing factor of porosity and effective stress of gas-filled coal. *Rock Soil Mech.* **2010**, *31*, 3417–3422. [CrossRef]